Research Square

Preprints are preliminary reports that have not undergone peer review.
They should not be considered conclusive, used to inform clinical practice,
or referenced by the media as validated information.

RF-Assisted EABC–PSO for Multi-UAV Collaborative Path Planning in Port Ship Emission Monitoring

Lizhi Huang
Zhejiang Wanli University
Jun Li
lijunreed@163.com
Zhejiang Wanli University
Xinyi Huang
Zhejiang Wanli University
Yubo Shao
Zhejiang Wanli University
Jiaxin Chen
Zhejiang Wanli University

Article

Keywords: Ship emission monitoring, Particle swarm optimization, Artificial bee colony algorithm, multi-UAV path planning, Random Forest, surrogate-assisted metaheuristics

Posted Date: November 23rd, 2026

DOI: https://doi.org/10.21203/rs.3.rs-11593827/v1

License: This work is licensed under a Creative Commons Attribution 4.0 International License.
Read Full License

Additional Declarations: No competing interests reported.

RF-Assisted EABC–PSO for Multi-UAV Collaborative Path Planning in Port Ship Emission Monitoring

Lizhi Huang [1], Jun Li [1,*], Xinyi Huang [1], Yubo Shao [1] and Jiaxin Chen [1]

[1]Zhejiang Wanli University, Ningbo 315100, China

*Correspondence: lijunreed@163.com

Abstract

Efficient inspection of spatially dispersed vessels requires coordinated routing of multiple unmanned aerial vehicles (UAVs). This study proposes a random forest (RF)-assisted enhanced artificial bee colony–particle swarm optimization (EABC-PSO) method to minimize total fleet flight distance and maximum individual task completion time in port ship emission monitoring. The proposed method embeds personal best and global best guidance into discrete vessel-assignment updates during the Employed Bee and Onlooker Bee Phases. Nearest-neighbor construction and 2-opt refinement determine each UAV's visiting sequence, while an offline random forest surrogate recommends parameter configurations. In the Ningbo Port and Shanghai Port scenarios constructed from automatic identification system (AIS) data, five-fold cross-validation yields mean R^2 values of 0.9643 and 0.9681, respectively. Relative to the balanced parameter configuration, RF-recommended settings reduce mean normalized fitness by 1.77% and 2.01%, respectively. Across 100 independent runs per algorithm and scenario, EABC-PSO achieves the lowest mean normalized fitness and shortest mean total flight distance in both scenarios. Compared with ABCO-PSO, PSO+TS, and IHGPA, its mean normalized fitness decreases by 19.09%, 19.30%, and 49.26% in the Ningbo Port scenario and by 15.37%, 22.18%, and 49.44% in the Shanghai Port scenario, respectively. Further experiments with three to seven UAVs identify four and five UAVs as the preferred fleet sizes among those tested for the Ningbo Port and Shanghai Port scenarios under equal objective weights. The proposed framework supports route optimization, parameter configuration, and fleet-size selection for port ship emission monitoring.

Keywords: Ship emission monitoring; Particle swarm optimization; Artificial bee colony algorithm; multi-UAV path planning; Random Forest; surrogate-assisted metaheuristics

1. Introduction

Maritime shipping is a major pillar of international trade and the global economy, accounting for more than 80% of global merchandise trade by volume [1]. As maritime activity continues to expand, emissions of sulfur oxides (SO_x), nitrogen oxides (NO_x), and particulate matter (PM) from ships during navigation, anchoring, and berthing pose growing threats to air quality in ports and surrounding coastal

cities. A previous review identified ships and harbour activities as important sources of particulate and gaseous pollutants and indicated that they may increase the exposure of coastal populations [2]. Ship emissions originate from dispersed sources, vary in duration, and are influenced by vessel operating conditions and weather. Port environmental management therefore requires not only an assessment of regional pollution but also timely identification and targeted monitoring of emissions from individual vessels.

Unmanned aerial vehicles equipped with lightweight sensors offer a practical platform for obtaining emission measurements from individual vessels. Yang et al. [3] evaluated a microsensor sniffing system carried by a UAV through field measurements in Hong Kong waters and demonstrated its applicability to estimating marine fuel sulfur content from ship exhaust. Šaparnis et al. [4] reviewed multirotor UAV measurements of gaseous and particulate emissions, documenting their application to individual vessels. These studies establish the feasibility of using UAVs to monitor ship emissions and provide a technical basis for extending individual inspection tasks to coordinated monitoring of multiple vessels.

Extending this monitoring capability to spatially dispersed vessels requires decisions on target assignment and visiting order, together with appropriate measures of operational performance. Shen et al. [5] minimized the duration of a coordinated monitoring operation, accounting for mothership travel, waiting, and UAV charging. Qi et al. [6] minimized cumulative UAV flight time under energy constraints. For a given fleet size, fixed cruising speed, and fixed acceleration and deceleration parameters, the latter objective is equivalent to minimizing total flight distance. However, minimizing cumulative flight distance does not necessarily minimize the time at which the last UAV completes its assigned tasks. Shortening this completion time may require reallocating targets among UAVs, potentially increasing total travel. These considerations motivate the joint evaluation of total fleet flight distance and maximum individual task completion time. Ma et al. [7] incorporated both total flight distance and mission completion time into cooperative task allocation for heterogeneous UAVs, illustrating the relevance of considering the two criteria together. For vessel inspection, total flight distance measures the aggregate travel required by the fleet, whereas maximum individual task completion time determines when all assigned inspections are finished. Balancing these criteria requires coordinated optimization of target allocation and the routes associated with each allocation.

Recent studies on UAV path planning and related routing problems have explored search guidance, solution representation, and local route improvement as complementary means of enhancing optimization performance. Ma et al. [8] introduced particle swarm optimization into the employed bee phase of the artificial bee colony algorithm to strengthen cooperative UAV trajectory search. Liu et al. [9] combined global search by PSO with local search by ABC for UAV planning in an urban airspace topology. Alongside these improvements to search guidance, Qi et al. [6] combined bee foraging learning and PSO with sequence

decoding, greedy route segmentation, and 2-opt improvement subject to energy constraints. Tong et al. [10] developed a hybrid ABC algorithm using population updates guided by pheromone information and a tensor representation for the multiple traveling salesman problem. These studies indicate that effective hybridization depends on coordinating candidate solution updates with the representation and refinement of routes. In cooperative vessel monitoring, reassigning a vessel changes the routes associated with the affected UAVs. Applying guidance from historical solutions therefore requires an update rule suited to discrete assignment variables, together with the construction and improvement of the routes resulting from each reassignment.

Beyond algorithm design, parameter configuration also influences the performance of hybrid swarm intelligence algorithms. Parameters governing the use of historically good solutions, population size, and abandonment can have interacting effects, making their joint selection more informative than examining each parameter separately. Configuration methods that use performance models address this issue by learning relationships between parameter settings and observed algorithm performance. Lindauer et al. [11] presented SMAC3, which supports configuration search using random forest performance models. Weiß et al. [12] developed Selector to combine multiple configuration suggesters and select candidates according to available evaluation resources. More recently, Anastacio et al. [13] accelerated configuration comparisons by using performance models to select informative instances, although improvements in the final configurations varied across solvers and benchmark scenarios. These advances address a common difficulty: configuration data must be obtained through actual algorithm executions, and reliable assessment of stochastic solvers may require repeated runs. Consequently, evaluating every joint parameter setting can become computationally demanding. A practical configuration approach must therefore exploit a limited set of evaluated settings to identify promising combinations within a substantially larger parameter domain.

Motivated by these requirements, this study proposes an RF-assisted EABC-PSO method for multi-UAV collaborative path planning in port ship emission monitoring. A routing model is formulated using vessel positions derived from automatic identification system (AIS) data, with a mothership serving as the common departure and return point. The model minimizes total fleet flight distance and maximum individual task completion time using a weighted sum of the normalized objectives, subject to complete target coverage, inspection duration, route closure, and UAV endurance requirements. EABC-PSO incorporates guidance inspired by the personal and global best memory mechanisms of PSO into updates to vessel assignments during the employed bee and onlooker bee phases. Scout bees replace stagnant solutions with randomly generated assignments to maintain population diversity. For each assignment, the nearest neighbor heuristic constructs initial routes, which are then refined using 2-opt to improve the visiting sequence of each UAV. An offline RF surrogate learns the relationship between parameter configurations and mean optimization performance, screens a larger candidate grid, and recommends settings separately for each port scenario. Experiments using vessel distributions from Ningbo Port and Shanghai Port first compare the RF-recommended parameter configurations with representative alternatives.

Using the recommended configuration for each port, EABC-PSO is then compared with baseline algorithms in terms of routing performance, convergence, and variability across independent runs, and evaluated across fleet sizes to examine the trade-off between flight distance and completion time.

2. Problem Description and Mathematical Model

2.1. Problem Description

The planning problem is formulated for a set of target vessels distributed across a designated port area, with vessel positions assumed to remain fixed during route planning. A fleet of UAVs operates from a mothership that remains stationary at a predetermined deployment location. Each target vessel must be inspected exactly once by one UAV, and each UAV must depart from and return to the mothership, forming a closed route. Here, vessel inspection refers to UAV-based sampling of ship exhaust plumes for emission monitoring. The associated measurement duration is modeled as a fixed service time at each vessel node. The planning decisions comprise vessel assignment and the visiting sequence of each UAV. These decisions are interdependent because the travel cost of serving a vessel depends on the other vessels assigned to the same UAV and their visiting order [14]. Each UAV's task completion time includes both flight time and the inspection time at its assigned vessels and must not exceed its endurance limit. The objective is to jointly minimize total fleet flight distance and maximum individual task completion time. Figure 1 illustrates the collaborative monitoring of ship emissions using multiple UAVs.

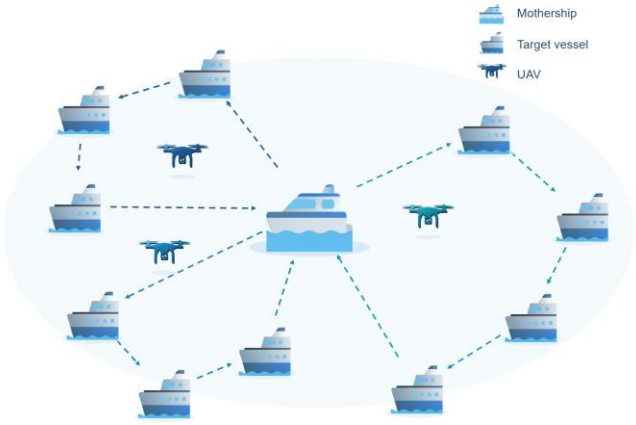


Figure 1. Illustration of multi-UAV cooperative monitoring of ship emissions.

2.2. Model Assumptions and Notations

In real-world port environments, the operational dynamics of utilizing UAVs to monitor ship emissions are inherently complex. To formulate a tractable mathematical model, the following assumptions are adopted in this study:

(1) The inspection duration for each target vessel by a UAV is a known constant.

(2) The mothership navigates to an optimal deployment location and remains stationary throughout the entire monitoring operation.

(3) All UAVs are deployed from the mothership, cruise at a constant speed, and return to their origin upon completion of their assigned monitoring missions.

(4) The impact of external environmental factors on the kinematic performance of the UAVs, mothership, and target vessels is considered negligible.

The notations employed in this paper are defined and summarized in Table 1.

Table 1. Summary of Mathematical Notations.

Notation	Description
0	Mothership node, used as the common departure and return depot.
S	Target-vessel set S = {1, 2, ..., N}, where N is the number of vessels.
V	Node set V = {0} ∪ S.
D	UAV set D = {1, 2, ..., K}.
A	Directed arc set A = {(i, j) ∈ V × V : i ≠ j}.
c_{ij}	Haversine distance between nodes i and j (km).
v	Common UAV cruising speed (km/h).
s	Fixed inspection duration for one vessel (min).
T_{lim}	Maximum permissible task completion time of one UAV (min).
P	Feasible nondominated pilot plans pooled across all fleet sizes compared within one port instance.
$\widehat{L}^{\text{I}}$	Estimated ideal value of total fleet flight distance (km).
$\widehat{L}^{\text{N}}$	Estimated nadir value of total fleet flight distance (km).
$\widehat{H}^{\text{I}}$	Estimated ideal value of maximum individual task completion time (min).
$\widehat{H}^{\text{N}}$	Estimated nadir value of maximum individual task completion time (min).
ΔL	Fixed positive distance range: estimated nadir distance minus estimated ideal distance (km).
ΔH	Fixed positive time range: estimated nadir duration minus estimated ideal duration (min).
α, β	Positive dimensionless objective weights, with α + β = 1.
a_{id}	Binary assignment variable; 1 if vessel i is assigned to UAV d, and 0 otherwise.
x_{ijd}	Binary routing variable; 1 if UAV d travels directly from i to j, and 0 otherwise.
u_i^d	Continuous vessel-order variable for subtour elimination, bounded between 1 and N.
L_d	Closed-route flight distance of UAV d, including its return to the mothership (km).
n_d	Number of vessels assigned to UAV d.
T_d	Task completion time of UAV d, including flying and vessel inspection (min).
L_{total}	Total fleet flight distance (km).
H	Maximum individual UAV task completion time (min).
F	Dimensionless normalized weighted routing objective.

2.3. Mathematical Formulation of the Multi-UAV Cooperative Path Planning Model

For each UAV d, L_d, n_d, and T_d denote its flight distance, number of assigned vessels, and task completion time, respectively. Task completion time includes both flight time and vessel inspection time. Distances are expressed in kilometres and durations in minutes. The individual route metrics, total fleet flight distance L_{total}, and maximum individual task completion time H are calculated as follows:

$$L_d = \sum_{(i,j)\in A} c_{ij} x_{ijd}, \quad n_d = \sum_{i\in S} a_{id}, \quad \forall d \in D \tag{1}$$

$$T_d = \frac{60}{v} L_d + s n_d, \quad \forall d \in D \tag{2}$$

$$L_{\text{total}} = \sum_{d\in D} L_d, \quad H = \max_{d\in D} T_d \tag{3}$$

Total fleet flight distance and maximum individual task completion time differ in units and numerical scale. Ideal–nadir range normalization expresses each objective as its deviation from an ideal reference value divided by the corresponding ideal–nadir range [15]. For a minimization problem, the ideal point comprises the minimum attainable value of each objective over the feasible set, whereas the nadir point comprises the maximum value of each objective over the Pareto optimal set. These reference points are generally unknown and are therefore estimated through a separate calibration stage.

Calibration is conducted separately for the Ningbo Port and Shanghai Port instances using the same balanced EABC-PSO configuration: $w = 0.70$, $c_1 = c_2 = 1.50$, 30 food sources, and an abandonment limit of 10. Within each port instance, the vessel positions, mothership location, UAV cruising speed, inspection duration, and endurance limit remain fixed. For each fleet size $K \in \{3,4,5,6,7\}$, EABC-PSO is run separately to minimize total fleet flight distance and maximum individual task completion time. Each objective is optimized over five repetitions, with 300 iterations per run, giving $5 \times 2 \times 5 = 50$ calibration runs per port. The calibration uses random seeds distinct from those used in the formal experiments.

Each calibration run contributes its final best plan, for which both objective values are recorded. The plans are pooled across the five fleet sizes within each port. Infeasible plans and duplicate objective pairs are removed, and the remaining plans are filtered according to dominance in the two objectives. A plan dominates another if neither objective is greater and at least one is strictly smaller. Let P denote the resulting nondominated pilot set and q a plan in P, with $H(q)$ representing the maximum task completion time among its UAVs. The estimated ideal and nadir reference values are defined as follows:

$$\hat{L}^{\mathrm{I}} = \min_{q\in P} L_{\text{total}}(q), \quad \hat{L}^{\mathrm{N}} = \max_{q\in P} L_{\text{total}}(q) \tag{4}$$

$$\hat{H}^{\mathrm{I}} = \min_{q\in P} H(q), \quad \hat{H}^{\mathrm{N}} = \max_{q\in P} H(q) \tag{5}$$

The hats denote estimates derived from the finite pilot set P. These values establish a common empirical reference range for comparisons across the tested fleet sizes within each port instance. The

components of an estimated reference point may originate from different plans. The corresponding normalization ranges are defined as follows:

$$\Delta L = \hat{L}^{\mathrm{N}} - \hat{L}^{\mathrm{I}} > 0, \quad \Delta H = \hat{H}^{\mathrm{N}} - \hat{H}^{\mathrm{I}} > 0 \tag{6}$$

Normalization requires a nonempty feasible pilot set and strictly positive reference ranges. If either range is zero or numerically negligible, the calibration must be reassessed before normalization is applied. Once established, the reference values and their corresponding ranges are saved and held fixed throughout the subsequent experiments for that port. The same saved values are used to generate RF training data, compare parameter configurations and algorithms, and evaluate different fleet sizes. Ningbo Port and Shanghai Port retain their respective reference values. Formal results outside the estimated ranges are retained without clipping, so normalized objective values may be negative or greater than one.

The model minimizes the weighted sum of normalized total fleet flight distance and maximum individual task completion time. The dimensionless weights satisfy $\alpha > 0, \beta > 0$ and $\alpha + \beta = 1$. Unless otherwise stated, equal weights, α = β = 0.5, are used in the experiments. Both the weights and the normalization reference values remain fixed during optimization. The objective function is formulated as follows:

$$\min F = \alpha \frac{L_{\mathrm{total}} - \hat{L}^{\mathrm{I}}}{\Delta L} + \beta \frac{H - \hat{H}^{\mathrm{I}}}{\Delta H} \tag{7}$$

Subject to:

$$\sum_{d \in D} a_{id} = 1, \quad \forall i \in S \tag{8}$$

$$\sum_{j \in V \setminus \{i\}} x_{ijd} = \sum_{j \in V \setminus \{i\}} x_{jid} = a_{id}, \quad \forall i \in S, d \in D \tag{9}$$

$$\sum_{j \in S} x_{0jd} = \sum_{i \in S} x_{i0d} = 1, \quad \forall d \in D \tag{10}$$

$$T_d = \frac{60}{v} L_d + sn_d \leq T_{\mathrm{lim}}, \quad \forall d \in D \tag{11}$$

$$u_i^d - u_j^d + N x_{ijd} \leq N - 1, \quad \forall i, j \in S, i \neq j, d \in D \tag{12a}$$

$$u_i^d \in \mathbb{R}, \quad 1 \leq u_i^d \leq N, \quad \forall i \in S, d \in D \tag{12b}$$

$$x_{ijd} \in \{0,1\}, \quad \forall (i,j) \in A, d \in D \tag{13a}$$

$$a_{id} \in \{0,1\}, \quad \forall i \in S, d \in D \tag{13b}$$

Constraint (8) assigns each vessel to exactly one UAV. Constraint (9) links vessel assignment to route selection and ensures one incoming and one outgoing arc for every vessel assigned to a UAV. Constraint (10), together with the exclusion of self-loops, requires each UAV to depart from and return to

the mothership, resulting in exactly K nonempty missions. Constraint (11) limits the total task completion time of each UAV, including both flight and inspection time; the factor 60 converts flight time from hours to minutes.

Constraints (12a)–(12b) eliminate subtours among target vessels using continuous order variables bounded between 1 and N [16]. Constraints (13a)–(13b) define the binary domains of the assignment and routing variables. Together, these constraints ensure that each UAV follows a single closed route through its assigned vessels.

At a fixed cruising speed, the endurance constraint implies $L_d \leq \frac{v}{60}(T_{\lim} - sn_d)$, thereby limiting the flight distance according to the inspection workload of each UAV. A separate maximum range constraint is needed only if an additional equipment range limit is specified. The estimated reference values are used exclusively for objective normalization and do not define feasibility bounds. Equation (7) evaluates feasible plans, while infeasible candidates are handled through penalties during heuristic search.

3. Algorithm Design

3.1. Particle Swarm Optimization

PSO is a nature-inspired metaheuristic algorithm based on swarm intelligence, simulating the social foraging behavior of bird flocks. In this framework, each candidate solution is conceptualized as a particle that navigates the multidimensional search space. A particle dynamically updates its position and velocity by tracking both its personal historical best position and the global best position discovered by the entire swarm. For the i-th particle, the velocity and position update equations are formulated as follows [17]:

$$v_i^{t+1} = w \cdot v_i^t + c_1 \cdot r_1 \cdot (pbest_i - x_i^t) + c_2 \cdot r_2 \cdot (gbest - x_i^t) \tag{14}$$

$$x_i^{t+1} = x_i^t + v_i^{t+1} \tag{15}$$

In the aforementioned equations, v_i^t denotes the velocity vector of particle *i* at iteration *t*, and x_i^t denotes its corresponding position vector. The parameter w represents the inertia weight, while c_1 and c_2 are the cognitive and social acceleration coefficients, respectively. The terms r_1 and r_2 are random variables uniformly distributed over the interval [0,1]. Furthermore, $pbest_i$ and $gbest$ refer to the historical personal best position achieved by particle i and the global best position identified by the swarm, respectively.

3.2. Artificial Bee Colony Algorithm

The ABC algorithm, developed by Karaboga and Basturk [18], is a swarm intelligence metaheuristic inspired by the cooperative foraging behavior of honeybee colonies. Its core principle lies in mapping potential candidate solutions within the solution space to virtual food sources, and achieving

global optimization through the division of labor and information sharing among three types of bees: employed bees, onlooker bees, and scout bees.

The specific search mechanism operates as follows: employed bees conduct local exploitation in the neighborhood of their currently assigned food sources and share information on the locations and nectar amounts of the food sources through an information-sharing mechanism. Subsequently, onlooker bees evaluate the transmitted fitness information and utilize a roulette wheel selection mechanism to probabilistically choose high-quality food sources for further intensive exploitation. Meanwhile, scout bees conduct random global exploration across the solution space to maintain population diversity and discover entirely new regions.

The algorithm effectively balances exploration and exploitation through a dynamic “recruitment and abandonment” mechanism. Specifically, “recruitment” occurs when onlooker bees are probabilistically directed to high-potential food sources based on their relative fitness values. Conversely, “abandonment” is triggered when a food source shows no fitness improvement over a predefined number of consecutive iterations (known as the "limit" parameter); such an “exhausted” source is abandoned, and its employed bee becomes a scout bee to generate a new random food source. Operating synergistically, these processes ensure the intensive exploitation of high-quality solutions while mitigating premature convergence. By eliminating stagnant solutions and injecting stochastic diversity, the ABC algorithm facilitates a highly robust search within the global solution space.

3.3. Enhanced Artificial Bee Colony-Particle Swarm Optimization Algorithm

Multi-UAV cooperative path planning is an NP-hard combinatorial optimization problem with coupled constraints and objectives. This study proposes an enhanced ABC-PSO algorithm for multi-UAV cooperative path planning in port ship emission monitoring.

EABC-PSO retains the employed bee, onlooker bee, and scout bee phases of the traditional ABC algorithm. During the employed bee and onlooker bee phases, personal and global best solutions guide updates to vessel assignments. Scout bees replace stagnant solutions with randomly generated assignments to maintain population diversity. For each assignment, the nearest neighbor heuristic constructs an initial route for each UAV, and 2-opt local search refines its visiting sequence during fitness evaluation. The algorithm is compared with selected baselines in terms of the normalized weighted objective, total flight distance, maximum individual task completion time, and convergence behavior.

3.3.1. Neighborhood Search Strategy Based on Particle Swarm Optimization

The EABC-PSO algorithm reduces the reliance of traditional ABC neighborhood search on purely stochastic perturbations by introducing the individual-global memory concept from PSO. The personal best solution (pbest) preserves food-source-level historical information, whereas the global best solution (gbest)

provides population-level guidance. Their effect on convergence efficiency is assessed empirically in Section 4.3.

The core mechanism is formulated as follows. Let *N* denote the length of the solution vector, representing the total number of target vessels. The *i*-th food source is defined as $x_i = (x_{i,1}, x_{i,2}, \ldots, x_{i,N})$, where $x_{i,j} \in \{1,2,\ldots,k\}$ indicates that the *j*-th vessel is assigned to the $x_{i,j}$-th UAV. During the generation of a new solution x_i', the value of each dimension j is determined using the following two-stage probabilistic rule derived from PSO:

$$x'_{i,j} = \begin{cases} x_{i,j} & r_0 < w \text{ or } a+b=0 \\ \text{pbest}_{i,j} & r_0 \geq w, r_3 < \frac{a}{a+b} \\ \text{gbest}_j & r_0 \geq w, r_3 \geq \frac{a}{a+b} \end{cases} \quad (16)$$

Here, w denotes the inertia weight, and c_1 and c_2 represent the cognitive and social acceleration coefficients, respectively. The variables r_0, r_1, r_2, and r_3 are mutually independent random numbers uniformly distributed over [0, 1]. Define $a = c_1 r_1$ and $b = c_2 r_2$. The current assignment is retained when $r_0 < w$. Otherwise, the dimension inherits its value from either the personal best solution or the global best solution, with relative selection probabilities $\frac{a}{a+b}$ and $\frac{b}{a+b}$, respectively.

This two-stage mechanism allows each dimension to retain its current assignment or inherit information from pbest or gbest. After all dimensions have been updated, a mutation is performed with probability $p_m = 0.1$. One dimension is selected uniformly at random and reassigned a UAV index drawn uniformly from $\{1,2,\ldots,K\}$. This mutation introduces variation into vessel assignments and helps maintain population diversity.

3.3.2. Path Optimization Using the Hybrid NNH-2-opt Strategy

In the final stage of path planning, a short visitation sequence must be constructed for the subset of vessels allocated to each UAV. Because visitation order determines route length and the resulting fitness value, local route improvement influences the algorithm's global search. A nearest-neighbor initialization followed by 2-opt refinement is therefore adopted.

Initially, the nearest-neighbor algorithm is employed to rapidly construct a feasible baseline route. Starting from the mothership, the algorithm iteratively selects the nearest unvisited vessel relative to the current position and appends it to the sequence before ultimately returning to the mothership to form a closed loop. This greedy construction is a standard traveling-salesman heuristic [19], but it can produce crossing edges and suboptimal detours. The nearest-neighbor construction is illustrated in Figure 2.

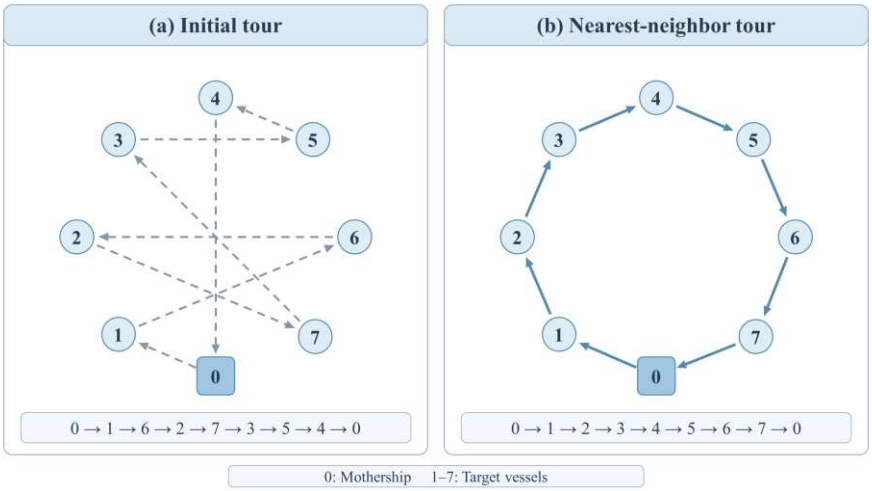


Figure 2. Illustration of closed path construction using the nearest neighbor heuristic.

To address these limitations, a 2-opt local optimization procedure refines the initial route by exchanging two non-adjacent edges to eliminate crossings and iteratively minimize the total distance [20]. Specifically, for a visitation sequence denoted as $\pi = (\pi_1, \pi_2, \ldots, \pi_n)$, the change in total distance associated with replacing edges $\mathrm{e}(\mathrm{p}_{\pi_i}, \mathrm{p}_{\pi_{i+1}})$ and $\mathrm{e}\left(p_{\pi_j}, p_{\pi_{j+1}}\right)$ with $\mathrm{e}\left(p_{\pi_i}, p_{\pi_j}\right)$ and $\mathrm{e}\left(p_{\pi_{i+1}}, p_{\pi_{j+1}}\right)$ is first evaluated. Only if the proposed exchange reduces the total distance is the subsequence from π_{i+1} to π_j reversed to implement the exchange. The process of exchanging edges continues until a local optimum is reached. Ultimately, this hybrid strategy effectively balances computational efficiency with optimization accuracy, yielding an improved visitation sequence for each UAV. An improving 2-opt move is illustrated in Figure 3.

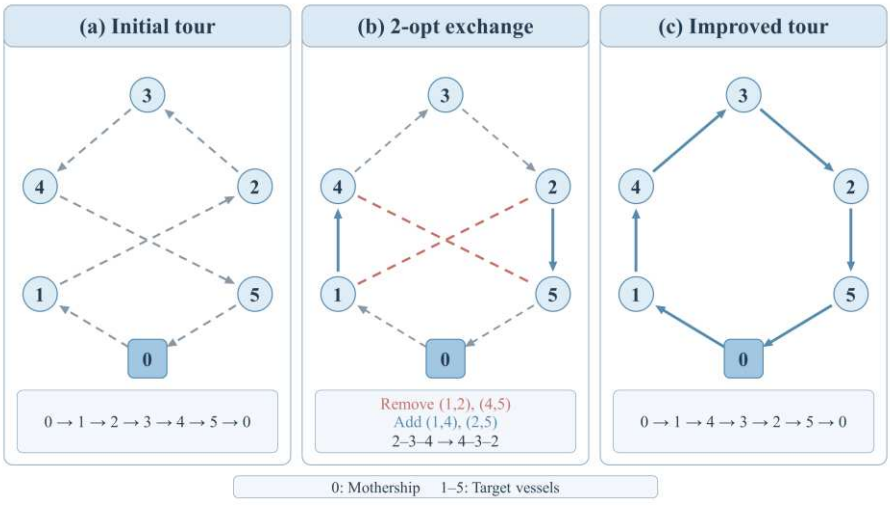


Figure 3. Illustration of a 2-opt edge exchange.

3.3.3. Overall Procedure of the EABC-PSO Algorithm

The overall procedure of the proposed EABC-PSO algorithm is illustrated in Figure 4. It consists of an initialization stage, three iterative evolutionary phases, and a termination assessment. The specific procedure is detailed as follows:

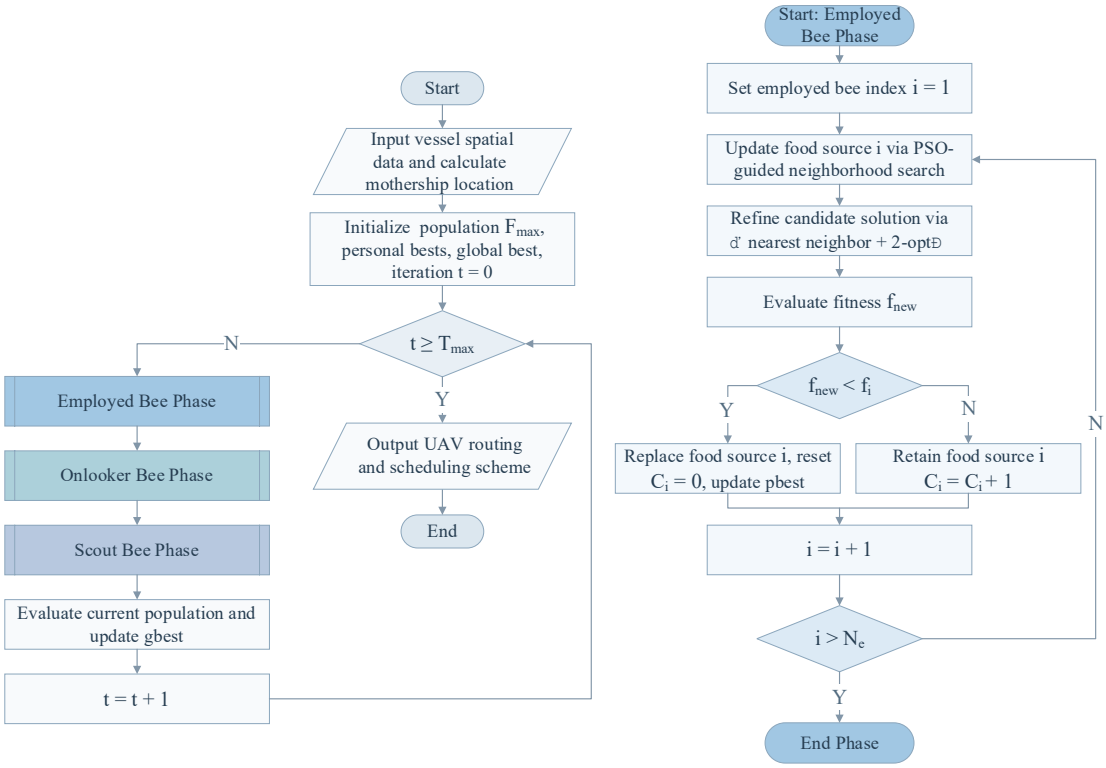
1) Initialization: A total of F_{max} food sources, representing initial solutions, are randomly generated within the search space. The fitness value of each food source is evaluated, and the personal best solution (pbest) of each food source and the global best solution (gbest) are initialized accordingly. Meanwhile, the abandonment counter C_i of each food source is set to zero, and the current iteration number is initialized as t = 0.

2) Employed Bee Phase: For each food source i, the employed bee generates a new candidate solution according to the PSO-based discrete mapping mechanism, in which pbest and gbest guide the search direction. Then, a hybrid nearest-neighbor and 2-opt local search strategy is applied to further improve the candidate solution, and its fitness value f_{new} is evaluated. Assuming a minimization objective, if $f_{new} < f_i$, greedy selection is performed: the original solution is replaced by the new candidate solution, the abandonment counter C_i is reset to zero, and pbest is updated if the new solution improves the historical best solution of the corresponding food source. Otherwise, the original solution is retained, and C_i is increased by one.

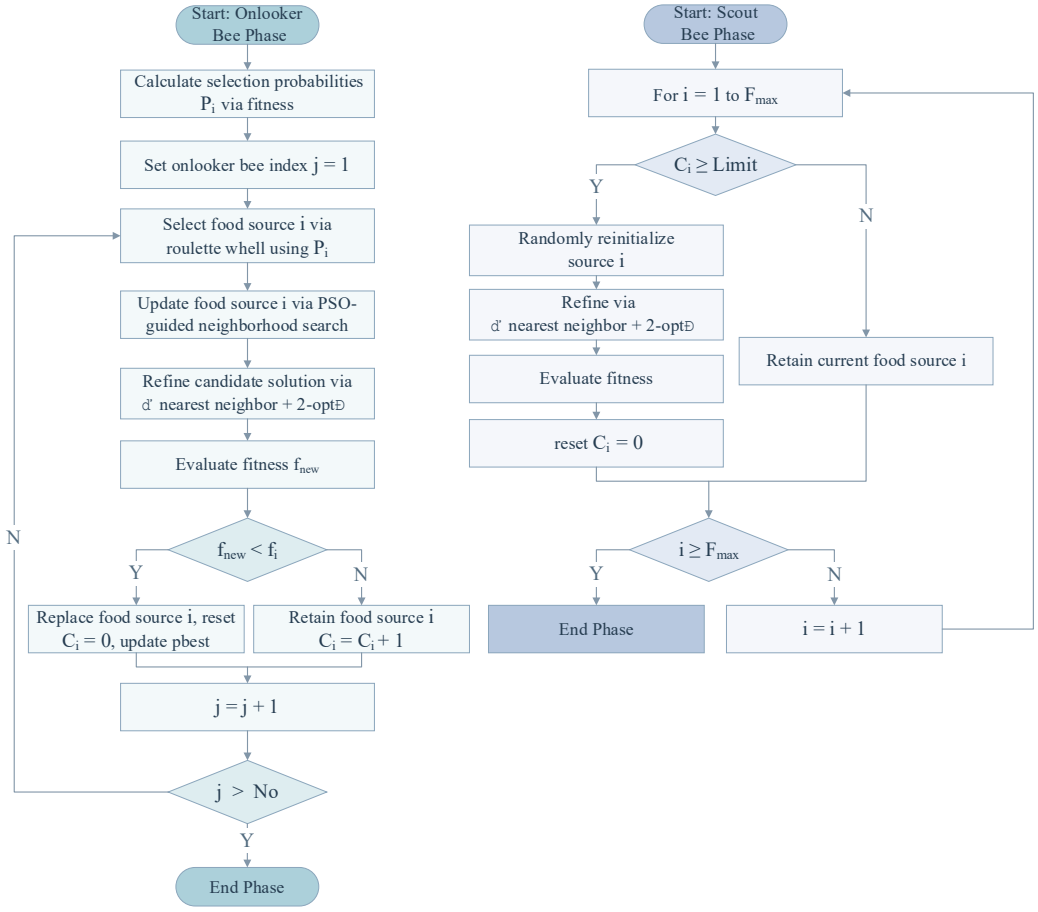
3) Onlooker Bee Phase: The selection probability P_i of each food source is calculated based on its normalized inverse fitness value. The onlooker bees then select food sources probabilistically using a roulette wheel selection. For the selected food sources, they subsequently perform the same candidate generation, local search, greedy selection, and update the abandonment counter using the same procedures as in the employed bee phase.

4) Scout Bee Phase: To alleviate premature convergence and escape from local optima, the algorithm checks whether any food source has stagnated. If the abandonment counter C_i of a food source exceeds or reaches the predefined threshold Limit, the corresponding employed bee is converted into a scout bee. The stagnant food source is randomly reinitialized and further refined using the same hybrid local search strategy to introduce stochastic diversity into the population. Its fitness value is then reevaluated, the abandonment counter is reset to zero, and pbest is updated only if the new solution improves its historical best fitness.

5) Global Best Update and Termination: After the three evolutionary phases, all updated food sources are examined, and gbest is updated once a better solution is found. The iteration counter is then increased as t = t + 1. Finally, the termination criterion is checked. If $t \geq T_{max}$, the iterative process terminates and returns gbest as the best solution found; otherwise, the algorithm returns to the employed bee phase for the next iteration.


Start
Input vessel spatial data and calculate mothership location
Initialize population F_{max}, personal bests, global best, iteration t = 0
$t \geq T_{max}$
N
Y
Employed Bee Phase
Onlooker Bee Phase
Scout Bee Phase
Evaluate current population and update gbest
t = t + 1
Output UAV routing and scheduling scheme
End
Start: Employed Bee Phase
Set employed bee index i = 1
Update food source i via PSO-guided neighborhood search
Refine candidate solution via ď nearest neighbor + 2-optĐ
Evaluate fitness f_{new}
$f_{new} < f_i$
Y
N
Replace food source i, reset $C_i = 0$, update pbest
Retain food source i $C_i = C_i + 1$
i = i + 1
$i > N_e$
N
Y
End Phase

333


Start: Onlooker Bee Phase
Calculate selection probabilities P_i via fitness
Set onlooker bee index j = 1
Select food source i via roulette whell using P_i
Update food source i via PSO-guided neighborhood search
Refine candidate solution via ď nearest neighbor + 2-optĐ
Evaluate fitness f_{new}
$f_{new} < f_i$
Y
N
Replace food source i, reset $C_i = 0$, update pbest
Retain food source i $C_i = C_i + 1$
j = j + 1
j > No
N
Y
End Phase
Start: Scout Bee Phase
For i = 1 to F_{max}
$C_i \geq$ Limit
Y
N
Randomly reinitialize source i
Refine via ď nearest neighbor + 2-optĐ
Evaluate fitness
reset $C_i = 0$
Retain current food source i
$i \geq F_{max}$
Y
N
End Phase
i = i + 1

334

Figure 4. Flowchart of the proposed EABC-PSO algorithm.

3.4. Parameter Recommendation Method Using an RF Surrogate Model

The routing quality obtained by EABC-PSO depends on the configuration of its control parameters. To reduce the cost of evaluating a large candidate grid through repeated algorithm runs, an offline RF surrogate is used to learn the relationship between parameter settings and observed algorithm performance [11,21]. The resulting workflow comprises data generation, surrogate training, parameter screening and validation, as illustrated in Figure 5.

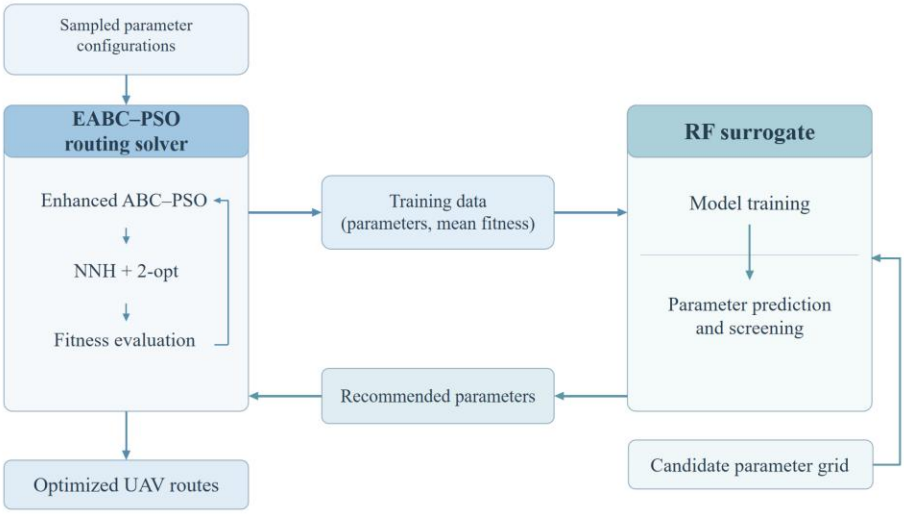


Figure 5. Interaction between EABC-PSO and the RF surrogate.

The configuration vector is $\theta = (w, c_1, c_2, F_{\max}, \text{Limit})$. The first three parameters govern the assignment updates in Eq. (16): w controls the retention of current assignments, while c_1 and c_2 jointly determine the relative probabilities of inheriting assignments from pbest and gbest. The parameter $F_{\max}$, denoted Food_num in the implementation, specifies the number of food sources, whereas Limit specifies the abandonment threshold for stagnant food sources. The candidate parameter values listed in Table 2 define the grid Θ, which includes only combinations satisfying $c_1 + c_2 \leq 4$.

Table 2. Preset parameter ranges for RF-assisted configuration screening.

Parameter	Symbol	Start Value	End Value	Step Size	Constraint
Inertia weight	w	0.1	1.00	0.05	-
Cognitive learning factor	c_1	0.25	4.00	0.25	c1 + c2 ≤ 4
Social learning factor	c_2	0.25	4.00	0.25	c1 + c2 ≤ 4
Number of food sources	$F_{\max}$	10	80	5	-
Scout-bee trigger threshold	Limit	5	50	5	-

Training data are generated separately for Ningbo Port and Shanghai Port by sampling configurations without replacement from Θ. For each sampled configuration i in port scenario σ ∈ {Ningbo Port, Shanghai Port}, EABC-PSO is run R times with independent random seeds under a common fleet size and stopping criterion. The performance response is the mean evaluation value of the plans returned by these runs:

$$y_{\sigma,i} = \frac{1}{R}\sum_{r=1}^{R} F_{\sigma}(q_{\sigma,i,r}) \tag{17}$$

Here, $q_{\sigma,i,r}$ denotes the best plan returned by run r for configuration i in port σ. For feasible plans, F_{σ} is the objective defined by ideal and nadir normalization in Eq. (7); infeasible candidates are evaluated using the constraint penalty rule of EABC-PSO. The normalization references and objective weights are fixed within each port scenario and are shared by all configurations in the corresponding training and comparison experiments. Averaging repeated runs limits the influence of stochastic variation on configuration assessment.

Separate RF regression models are fitted for the two ports using the configuration vectors as inputs and the mean observed evaluation values in Eq. (17) as responses. Each model combines regression trees trained on resampled observations and randomized feature subsets [22]. Let $h_{\sigma,b}$ denote tree b in the model for scenario σ and B the number of trees. The predicted response for a configuration is obtained by averaging the tree outputs:

$$\hat{y}_{\sigma}(\theta) = \frac{1}{B}\sum_{b=1}^{B} h_{\sigma,b}(\theta) \tag{18}$$

The fitted model for each port predicts the mean evaluation value of every configuration in Θ. The configuration with the lowest predicted value is selected as the recommendation:

$$\theta_{\sigma}^{\mathrm{RF}} \in \arg\min_{\theta\in\Theta} \hat{y}_{\sigma}(\theta) \tag{19}$$

The recommended configuration is returned to EABC-PSO for repeated runs, and its effectiveness is assessed from the resulting routing performance under the same evaluation protocol as the comparison configurations. Consistent with the distinction between surrogate predictions and actual evaluations [23], RF is used for parameter screening, while candidate route objectives are calculated explicitly throughout EABC-PSO search. The RF settings, predictive accuracy and validation results are reported in Section 4.2.

4. Experiments and Analysis

Simulations were conducted with the objectives of minimizing the total flight distance of all UAVs and the maximum individual task completion time to evaluate the multi-UAV cooperative routing model for ship emission monitoring. The proposed EABC-PSO algorithm was compared with three baseline

algorithms. The hybrid artificial bee colony optimization and particle swarm optimization baseline, denoted ABCO-PSO, followed the multiobjective tour-routing method proposed by Beed et al. [24]. The particle swarm optimization and tabu search baseline, denoted PSO+TS, followed the multi-UAV path-planning method proposed by Wang [25]. The improved hybrid genetic particle swarm algorithm baseline, denoted IHGPA, followed the UAV path-planning method proposed by Wu et al. [26].

The experiments were implemented using MATLAB R2024b and PyCharm 2025.1.3.1 and conducted on a workstation equipped with an Intel(R) Core(TM) i5-13400F CPU operating at 2.50 GHz and 32 GB of RAM. All stochastic comparisons were performed over 100 independent runs, and all compared algorithms were evaluated using a consistent computational budget, stopping criterion, and parameter-reporting protocol. Normalization bounds were specified separately for Ningbo Port and Shanghai Port and were kept consistent across all compared algorithms within each port.

4.1. Data Preparation

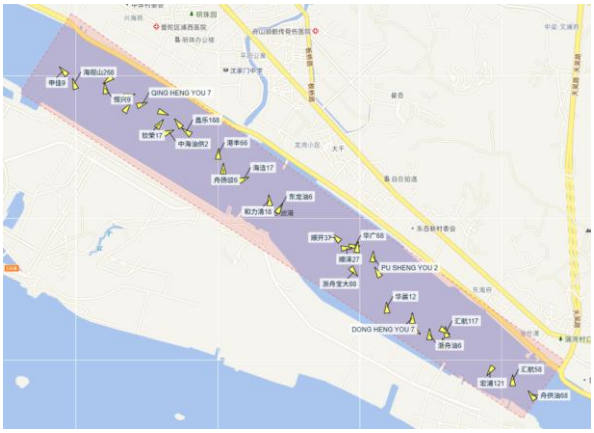


Figure 6. Geographic distribution of target vessels in Ningbo Port.



Figure 7. Geographic distribution of target vessels in Shanghai Port.

The subsequent experiments employed anchored vessels at Ningbo Port and Shanghai Port as the simulated monitoring targets. The real-world spatial data of these vessels were extracted from the Shipxy AIS platform. The vessel screening criteria were defined as follows: vessel types were strictly limited to cargo ships, container ships, and tankers; vessel length and flag were unrestricted; and the navigational status was required to be "anchored" with a speed of 0 knots.

Specifically, the monitoring area at Shanghai Port was delineated by four coordinate points (31°26.748'N 121°33.844'E, 31°24.621'N 121°31.702'E, 31°20.488'N 121°41.363'E, and 31°22.449'N 121°42.341'E), within which 29 target vessels (7 container ships and 22 cargo ships) were identified. Similarly, the monitoring area at Ningbo Port was defined by four coordinate points (29°58.117'N 122°14.013'E, 29°57.800'N 122°13.776'E, 29°56.491'N 122°16.109'E, and 29°56.725'N 122°16.299'E), yielding a total of 27 target vessels (1 cargo ship and 26 tankers).

Figures 6 and 7 show the geographic distributions of the target vessels in Ningbo Port and Shanghai Port, respectively. The vessels are numbered S_1 to S_{27} in Ningbo Port and S_{28} to S_{56} in Shanghai Port, with their coordinates listed in Table 3. Figures 8 and 9 present the two-dimensional scatter plots generated after the spatial coordinate transformation of the raw AIS data. Finally, Table 4 summarizes the main simulation parameters, with the single-vessel emission inspection duration fixed at 2 min following Shen et al. [27]. The resulting service time sn_d is added to flight time in Eq. (2) to calculate each UAV's task completion time and check its endurance constraint.

Table 3. Initial Coordinates of the Target Vessels.

Ship	Latitude	Longitude
S_1	29°57.864'N	122°14.004'E
S_2	29°57.770'N	122°14.367'E
S_3	29°57.683'N	122°14.389'E
⋮	⋮	⋮
S_{54}	31°21.607'N	121°40.969'E
S_{55}	31°21.755'N	121°41.169'E
S_{56}	31°21.520'N	121°41.378'E

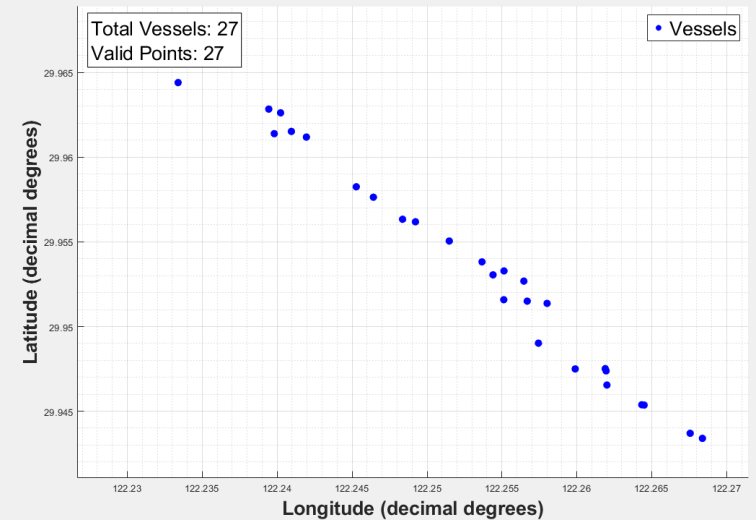


Figure 8. Scatter plot of the initial locations of target vessels in Ningbo Port.

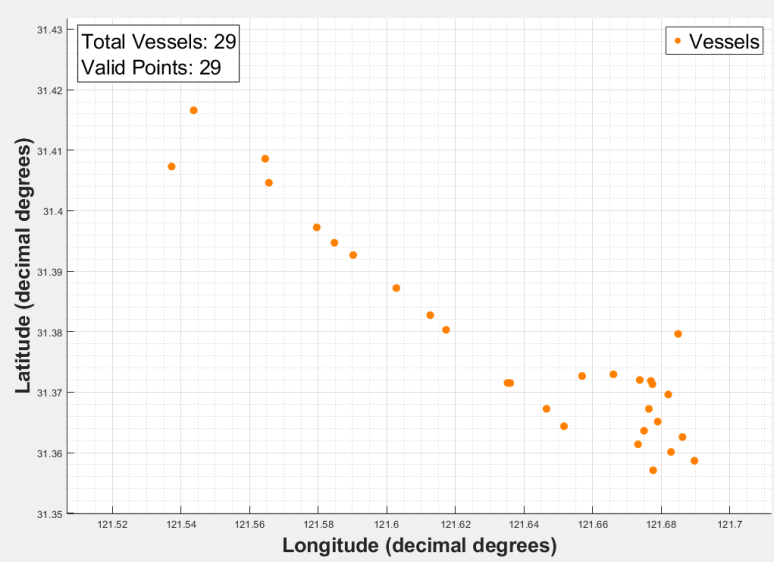


Figure 9. Scatter plot of the initial locations of target vessels in Shanghai Port.

Table 4. Simulation Parameter Configurations.

Simulation Parameter	Assigned Value
Average UAV cruising speed	50 km/h
Average single vessel emission inspection duration	2 min/ship
Number of motherships	1
Maximum UAV endurance limit	51 min

4.2. RF Predictive Performance and Parameter Recommendation

4.2.1. RF Training and Predictive Performance

The configuration space follows Table 2. Its Cartesian product, restricted to $c_1 + c_2 \leq 4$, contains 342,000 candidate vectors. For each port, 2,000 vectors are sampled without replacement, and each configuration is evaluated in five independent EABC-PSO runs of 500 iterations to obtain its mean response. Random sampling is used to cover the preset configuration space [28]. The target response and the fixed normalization-reference protocol are defined in Section 3.4.

Each port-specific RF model contains 200 trees, with a maximum depth of 15 and a minimum of five samples per leaf; the remaining model settings retain their implementation defaults. Five-fold cross-validation is used to assess predictive performance. The mean coefficients of determination and their standard deviations across folds are:

$$R_{\text{Ningbo Port}}{}^2 = 0.964288 \pm 0.009574$$

$$R_{\text{Shanghai Port}}{}^2 = 0.968127 \pm 0.007122$$

The cross-validation scores for both ports exceed the surrogate-acceptance threshold of $R^2 = 0.8$, and both RF models are therefore accepted for parameter screening. Both port-specific models show good predictive performance within the sampled configuration data, with relatively small variation across folds. These scores assess configuration-performance prediction; they do not establish that the minimum predicted response is the true best configuration. Actual EABC-PSO runs are therefore used to evaluate the recommendations.

4.2.2. Performance of Configurations Recommended by RF

Applying the screening rule in Section 3.4 to all 342,000 candidates yields the recommended configuration (w, c1, c2, Food_num, Limit) = (0.90, 1.75, 1.75, 80, 10) for Ningbo Port and (0.80, 2.50, 0.25, 65, 30) for Shanghai Port. Table 5 lists these configurations together with five representative alternatives: balanced, high inertia and low cognitive, low inertia and high cognitive, large population, and small population configurations.

Each configuration is evaluated in 100 runs of 500 iterations with five UAVs and $\alpha = \beta = 0.5$. Within each port, all configurations use the same fixed normalization bounds determined using the balanced configuration (0.70, 1.50, 1.50, 30, 10), consistent with those used for RF training. Mean fitness and sample standard deviation are reported. Two-sided Welch's t-tests [29] compare the RF recommendation with each alternative at $\alpha = 0.05$. Negative t-statistics indicate a lower RF mean. Tables 6 and 7 report the Ningbo Port and Shanghai Port results, respectively.

In Ningbo Port, the RF-recommended configuration achieves a mean normalized fitness of 0.278395 ± 0.003787, compared with 0.283422 ± 0.006908 for the balanced configuration, a reduction of 1.77%. It has the lowest mean and standard deviation among the six configurations, with a standard deviation 45.17% below that of the balanced configuration. All five Welch comparisons yield $p < 0.0001$. The comparison with the balanced configuration gives $t = -6.3820$ and $p = 1.9615 \times 10^{-9}$, while that with the large-population configuration gives $t = -5.0685$ and $p = 9.7490 \times 10^{-7}$.

In Shanghai Port, the RF-recommended configuration achieves a mean normalized fitness of 0.288022 ± 0.007351, compared with 0.293938 ± 0.010428 for the balanced configuration, a reduction of 2.01%. It also has the lowest mean and standard deviation among the six configurations, with a standard deviation 29.51% below that of the balanced configuration. All five Welch comparisons are significant at the 0.05 level. The high-inertia and low-cognitive comparison yields $t = -3.4834$ and $p = 0.00061318$; the large-population comparison yields $t = -3.1324$ and $p = 0.00201454$. The other three comparisons yield $p < 0.0001$. These findings support RF selection relative to the tested alternatives under the fixed instances and evaluation protocol.

Table 5. Parameter configurations for Ningbo Port and Shanghai Port.

Parameter Configuration	Port	w	C_1	C_2	Food_num	Limit
Balanced Configuration	Both ports	0.7	1.5	1.5	30	10
High Inertia and Low Cognitive	Both ports	0.9	1.0	1.0	30	10
Low Inertia and High Cognitive	Both ports	0.4	2.0	2.0	30	10
Large Population	Both ports	0.7	1.5	1.5	50	15
Small Population	Both ports	0.7	1.5	1.5	15	5
RF-recommended	**Ningbo Port**	**0.90**	**1.75**	**1.75**	**80**	**10**
RF-recommended	**Shanghai Port**	**0.80**	**2.50**	**0.25**	**65**	**30**

Table 6. Statistical comparison of parameter configurations in Ningbo Port.

Parameter Configuration	Average Fitness	Standard Deviation	t-statistic	p-value (vs. RF Optimized)	Significance ($\alpha = 0.05$)
Balanced Configuration	0.2834	0.0069	-6.3820	<0.0001	Yes
High Inertia and Low Cognitive	0.2818	0.0062	-4.6927	<0.0001	Yes
Low Inertia and High Cognitive	0.3008	0.0177	-12.3667	<0.0001	Yes
Large Population	0.2816	0.0051	-5.0685	<0.0001	Yes
Small Population	0.2906	0.0121	-9.5789	<0.0001	Yes
RF-Optimized Configuration	**0.2784**	**0.0038**	**-**	**-**	**-**

Table 7. Statistical comparison of parameter configurations in Shanghai Port.

Parameter Configuration	Average Fitness	Standard Deviation	t-statistic	p-value (vs. RF Optimized)	Significance ($\alpha = 0.05$)
Balanced Configuration	0.2939	0.0104	-4.6375	<0.0001	Yes
High Inertia and Low Cognitive	0.2920	0.0088	-3.4834	0.0006	Yes
Low Inertia and High Cognitive	0.3020	0.0152	-8.2809	<0.0001	Yes
Large Population	0.2918	0.0095	-3.1324	0.0020	Yes
Small Population	0.2973	0.0123	-6.4460	<0.0001	Yes
RF-Optimized Configuration	**0.2880**	**0.0074**	-	-	-

4.3. Analysis of Experimental Results

4.3.1. Comparison of Algorithm Convergence

Figure 10 compares the mean convergence curves over 100 independent runs in the Ningbo Port scenario, using five UAVs, equal objective weights ($\alpha = \beta = 0.5$), and 500 iterations. The 95% reduction criterion refers to completing 95% of each mean curve's fitness decrease from its first recorded value to iteration 500.

EABC-PSO declines most sharply during the first 50 iterations and becomes nearly flat after approximately 200 iterations, reaching the 95% reduction criterion at iteration 121. ABCO-PSO also improves rapidly initially but shows a longer gradual decline, reaching the criterion at iteration 255. IHGPA exhibits only a shallow decrease after approximately 100 iterations and reaches the criterion at iteration 383. PSO+TS maintains a sustained decline through the middle and late stages, reaching the criterion at iteration 437 and approaching ABCO-PSO toward the end.

EABC-PSO achieves the lowest final mean fitness of approximately 0.28, compared with approximately 0.34 for ABCO-PSO and PSO+TS and 0.55 for IHGPA. These results indicate that EABC-PSO combines faster early improvement with better final solution quality among the four algorithms in the Ningbo Port scenario.

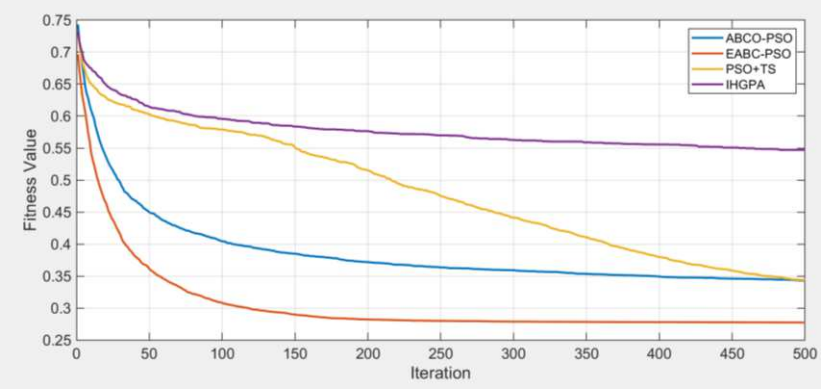


Figure 10. Mean convergence curves of the four algorithms in the Ningbo Port scenario.

4.3.2. Comparison of Algorithm Performance

Table 8 compares the four algorithms in the Ningbo Port scenario involving 27 target vessels. Five UAVs were deployed, both objective weights were set to 0.5, and each algorithm was independently executed 100 times with 500 iterations per run. The normalized fitness value, total flight distance, and maximum individual task completion time are reported as means with standard deviations.

EABC-PSO achieves the lowest mean fitness value of 0.2776 ± 0.0035 and the shortest total flight distance of 13.01 ± 0.67 km. Relative to ABCO-PSO, PSO+TS, and IHGPA, its mean fitness value is lower by approximately 19.09%, 19.30%, and 49.26%, respectively, while its total flight distance is reduced by 13.55%, 12.92%, and 32.45%. EABC-PSO also has the smallest standard deviations in fitness and flight distance, indicating more consistent results for these two metrics across the independent runs.

The maximum individual task completion time reveals a trade-off between the two objectives. EABC-PSO obtains 17.47 ± 0.93 min, slightly exceeding the 17.16 ± 1.05 min of ABCO-PSO and the 17.36 ± 1.17 min of PSO+TS, while remaining below the 19.54 ± 1.63 min of IHGPA. Thus, EABC-PSO provides the best normalized weighted objective in the Ningbo Port scenario primarily through its shorter total flight distance.

Table 8. Performance Comparison of the Four Algorithms under the Ningbo Port Scenario.

Algorithm	Fitness Value Mean ± Std.Dev.	Total Flight Distance (km) Mean ± Std.Dev.	Max Task Time (min) Mean ± Std.Dev.
EABC-PSO	**0.2776 ± 0.0035**	**13.01 ± 0.67**	**17.47 ± 0.93**
ABCO-PSO	0.3431 ± 0.0196	15.05 ± 0.83	17.16 ± 1.05
IHGPA	0.5471 ± 0.0352	19.26 ± 1.38	19.54 ± 1.63
PSO+TS	0.3440 ± 0.0311	14.94 ± 1.10	17.36 ± 1.17

To further verify the robustness of the proposed algorithm, an additional experiment was conducted using 29 target vessels from Shanghai Port, while all other simulation parameters remained unchanged. Compared with the Ningbo Port scenario, the Shanghai Port case covers a broader geographical area and presents a more heterogeneous vessel distribution, thereby increasing the difficulty of multi-UAV cooperative path planning.

As shown in Table 9, EABC-PSO achieves the lowest mean fitness value of 0.2880 ± 0.0075 in the Shanghai Port scenario, improving on ABCO-PSO, PSO+TS, and IHGPA by approximately 15.37%, 22.18%, and 49.44%, respectively. It also obtains the shortest total flight distance of 66.51 ± 4.69 km, corresponding to reductions of 6.31%, 5.89%, and 23.46% relative to the same three algorithms. These results show that the advantage in normalized fitness and route length is maintained in the broader port environment.

EABC-PSO also achieves the shortest maximum task time in Shanghai Port, at 35.43 ± 1.48 min, compared with 36.31 ± 1.43 min for ABCO-PSO, 37.55 ± 1.30 min for PSO+TS, and 41.10 ± 1.89 min for IHGPA. Unlike the small distance-time trade-off observed in Ningbo Port, EABC-PSO improves both mean flight distance and mean maximum task time in Shanghai Port. Its standard deviations in fitness and flight distance are also the smallest among the four algorithms, supporting the consistency of its results for these metrics across the two port scenarios.

Table 9. Performance Comparison of the Four Algorithms under the Shanghai Port Scenario.

Algorithm	Fitness Value Mean ± Std.Dev.	Total Flight Distance (km) Mean ± Std.Dev.	Max Task Time (min) Mean ± Std.Dev.
EABC-PSO	**0.2880 ± 0.0075**	**66.51 ± 4.69**	**35.43 ± 1.48**
ABCO-PSO	0.3403 ± 0.0244	70.99 ± 5.83	36.31 ± 1.43
IHGPA	0.5696 ± 0.0373	86.90 ± 6.48	41.10 ± 1.89
PSO+TS	0.3701 ± 0.0367	70.67 ± 6.53	37.55 ± 1.30

4.3.3. Performance analysis Across Different Fleet Sizes.

To evaluate performance across different fleet sizes, EABC-PSO was tested with 3–7 UAVs in the Ningbo Port and Shanghai Port scenarios, containing 27 and 29 target vessels, respectively. Each fleet size was evaluated over 100 independent runs with 500 iterations per run. Each port used its respective RF-recommended configuration from Section 4.2.2, with both objective weights set to 0.5. Within each port, all fleet sizes shared the same fixed ideal–nadir normalization references. Tables 10 and 11 report means and sample standard deviations calculated directly from the repeated-run results.

In Ningbo Port, Table 10 and Figure 11 show that the four-UAV configuration achieves the lowest mean normalized fitness of 0.2723 ± 0.0025. This represents reductions of 12.57%, 1.88%, 3.67%, and 6.26% compared with the configurations using three, five, six, and seven UAVs, respectively.

Further increasing the fleet size reduces the mean maximum task time but increases the mean total flight distance. From four to seven UAVs, the mean total flight distance increases by 15.24% to 14.33 ± 1.06 km, whereas the mean maximum task time decreases by 11.95% to 15.97 ± 1.53 min, resulting in a higher mean normalized fitness. Among the configurations using four to seven UAVs, the four-UAV configuration also has the smallest standard deviations for all three metrics. The three-UAV configuration has zero standard deviations at the reported precision, but its longer maximum task time leads to a higher mean normalized fitness. Figure 12 presents the routes from the best observed single run with four UAVs in Ningbo Port.

In Shanghai Port, Table 11 and Figure 13 show that the five-UAV configuration achieves the lowest mean normalized fitness of 0.2880 ± 0.0075, representing reductions of 11.30%, 2.01%, 0.43%, and 3.61% compared with the configurations using three, four, six, and seven UAVs, respectively.

Increasing the Shanghai Port fleet from five to seven UAVs raises the mean total flight distance by 7.02% to 71.18 ± 3.37 km, but reduces the mean maximum task time by only 2.23% to 34.64 ± 1.07 min. The resulting mean normalized fitness increases by 3.74%, indicating diminishing time benefits relative to the additional travel. Four UAVs provide the smallest standard deviation in normalized fitness, whereas five UAVs provide the lowest mean normalized fitness. The five- and six-UAV mean normalized fitness values differ by only 0.001236, which is small relative to their sample standard deviations. Thus, the preference for five UAVs follows the selection criterion based on mean normalized fitness. Figure 14 presents the routes from the best observed single run with five UAVs in Shanghai Port.

Overall, the results favor four UAVs in Ningbo Port and five UAVs in Shanghai Port among the tested fleet sizes under the stated weights and fixed normalization references. All tested configurations remain feasible, while their mean normalized fitness and between-run variability depend on fleet size and port geometry. Additional UAVs shorten mission completion time but require more travel on separate closed routes, so the preferred fleet size reflects a scenario-specific balance between these objectives.

Table 10. EABC-PSO performance across different fleet sizes in Ningbo Port.

Number of UAVs	Fitness Value Mean ± Std.Dev.	Total Flight Distance(km) Mean ± Std.Dev.	Max Task Time (min) Mean ± Std.Dev.
3	0.311475 ± 0.000000	10.600010 ± 0.000000	22.736608 ± 0.000000
4	**0.272334 ± 0.002503**	**12.432309 ± 0.108810**	**18.136948 ± 0.200005**
5	0.277554 ± 0.003496	13.005832 ± 0.667377	17.467774 ± 0.929758
6	0.282698 ± 0.003469	13.600473 ± 0.869399	16.762094 ± 1.253098
7	0.290530 ± 0.006097	14.326574 ± 1.062858	15.968827 ± 1.532794

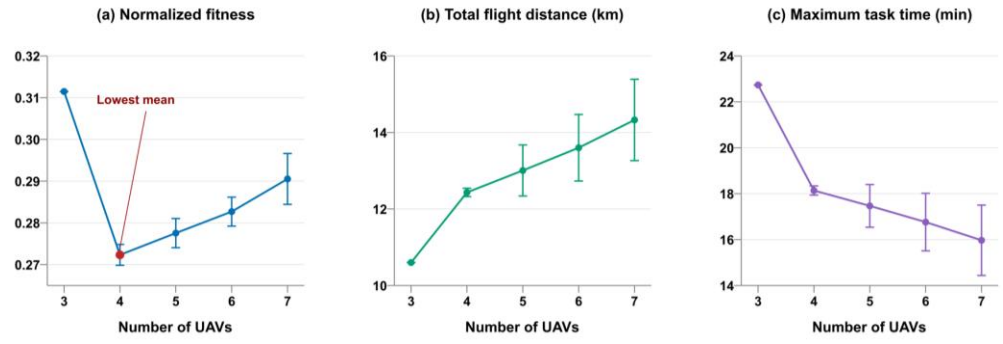


Figure 11. Effects of fleet size on EABC-PSO performance in Ningbo Port.

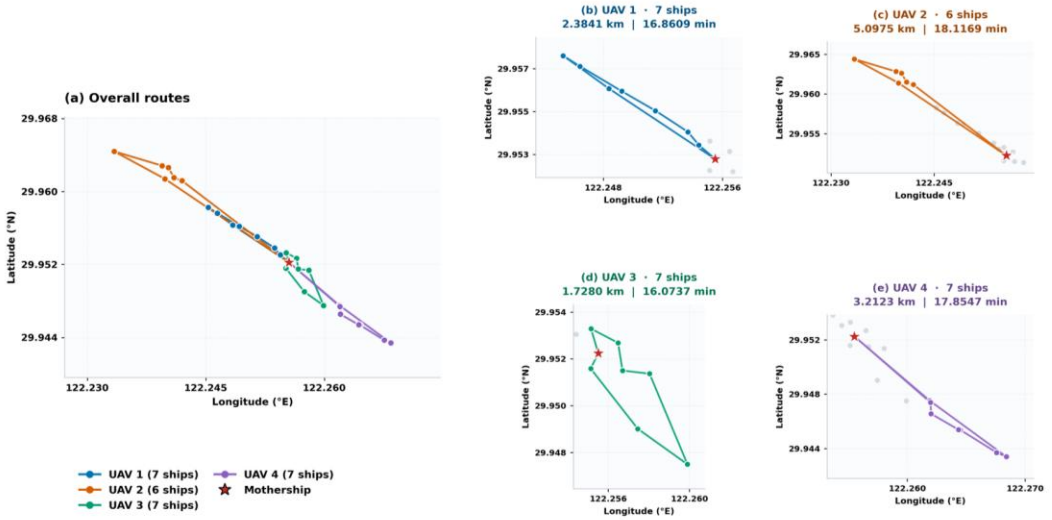


Figure 12. Flight routes for the preferred configuration of four UAVs in Ningbo Port.

Table 11. EABC-PSO performance across different fleet sizes in Shanghai Port.

Number of UAVs	Fitness Value Mean ± Std.Dev.	Total Flight Distance(km) Mean ± Std.Dev.	Max Task Time (min) Mean ± Std.Dev.
3	0.324642 ± 0.016100	51.550453 ± 0.846539	40.730513 ± 0.456470
4	0.293881 ± 0.001256	60.862751 ± 2.418017	37.125355 ± 0.665869
5	**0.287963 ± 0.007469**	**66.513683 ± 4.693265**	**35.432971 ± 1.478491**
6	0.289199 ± 0.009345	67.892720 ± 4.780490	35.124105 ± 1.498361
7	0.298743 ± 0.007886	71.183813 ± 3.366284	34.643160 ± 1.069736

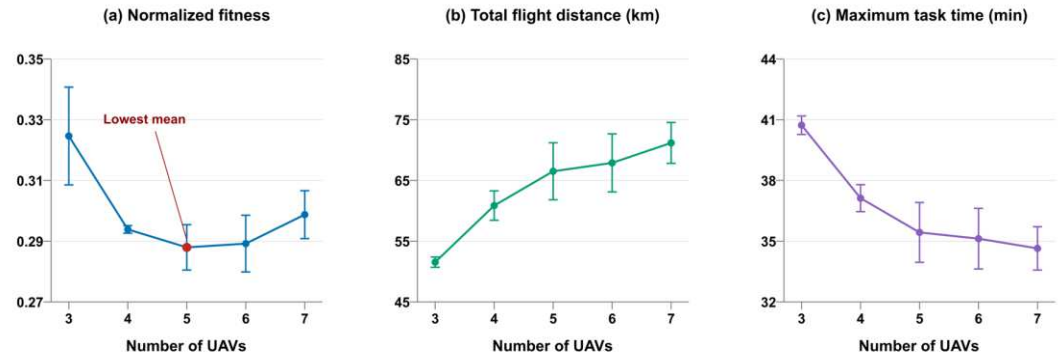


Figure 13. Effects of fleet size on EABC-PSO performance in Shanghai Port.

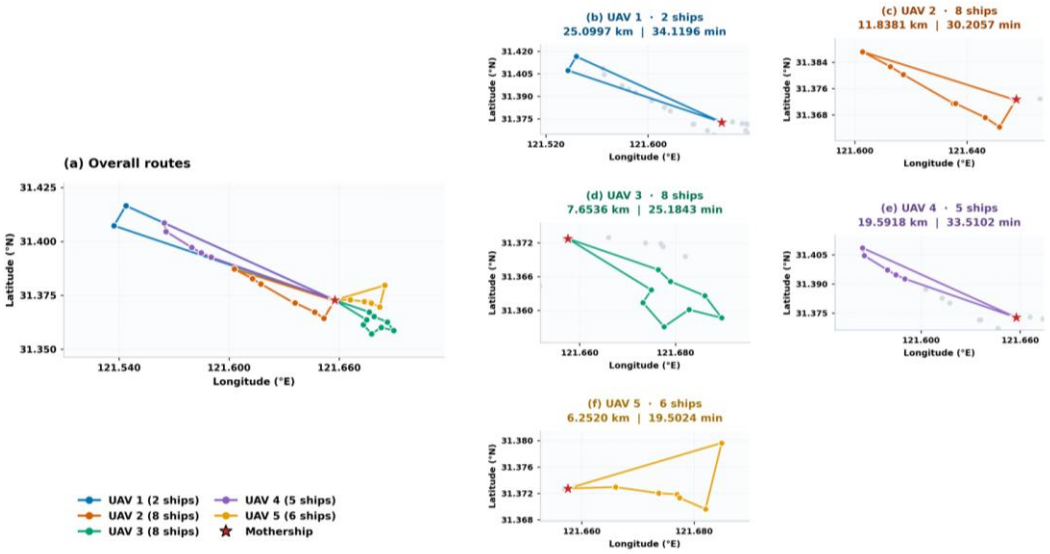


Figure 14. Flight routes for the preferred configuration of five UAVs in Shanghai Port.

5. Conclusions

This study developed an EABC-PSO method for multi-UAV collaborative path planning in port ship emission monitoring to jointly minimize total fleet flight distance and maximum individual task completion time. The method incorporated PSO-inspired personal best and global best guidance into discrete vessel-assignment updates during the Employed Bee and Onlooker Bee Phases of ABC. Combined with nearest-neighbor route construction and 2-opt refinement, this mechanism enabled coordinated optimization of vessel assignments and UAV visiting sequences.

To reduce dependence on empirical parameter tuning, RF surrogate models were used to learn the relationship between five control parameters and algorithm performance and to recommend configurations for the Ningbo Port and Shanghai Port scenarios. Cross validation using five folds yielded R^2 values of 0.9643 and 0.9681, respectively. In formal comparisons over 100 runs using fixed normalization references generated by the balanced configuration, the RF recommendations achieved lower mean normalized fitness than all five representative alternatives. Welch t tests assessed differences in either direction, and all comparisons were significant at an unadjusted significance level of 0.05.

In Ningbo Port, the configuration (0.90, 1.75, 1.75, 80, 10) achieved a mean normalized fitness of 0.278395 ± 0.003787, representing a reduction of 1.77% relative to the balanced configuration, with all five p values below 0.0001. In Shanghai Port, the configuration (0.80, 2.50, 0.25, 65, 30) achieved 0.288022 ± 0.007351, representing a reduction of 2.01% relative to the balanced configuration, with all five p values below 0.0021.

In algorithm comparisons over 100 runs, EABC-PSO achieved the lowest mean normalized fitness and shortest mean total flight distance in both port scenarios. Experiments on fleet size in Ningbo Port used 100 runs for each tested fleet size and identified four UAVs as the preferred configuration. The corresponding experiments in Shanghai Port favored five UAVs under the same selection criterion based on mean normalized fitness. These findings indicate that the appropriate fleet size depends on the spatial distribution of monitoring targets and the additional travel associated with repeated departures from and returns to the deployment point.

Overall, the proposed framework provides unified support for cooperative route optimization, parameter recommendation based on data, and UAV fleet configuration in ship emission monitoring missions across different port environments. The present study assumes anchored vessels, a stationary mothership, and homogeneous UAVs, while validation relies primarily on simulation. Future research should investigate online route adjustment for moving vessels and dynamic mothership operations and should evaluate the proposed method through field experiments and hardware-in-the-loop tests.

Data availability

The data that support the findings of this study are available from the corresponding author, Jun Li, upon reasonable request.

Author contributions

Lizhi Huang: Conceptualization, Methodology, Validation, Writing – original draft; **Jun Li**: Writing – review & editing, Supervision; **Xinyi Huang**: Formal analysis; **Yubo Shao**: Visualization, Data curation; **Jiaxin Chen**: Software, Data curation.

Competing interests

The authors declare no conflict of interest.

Funding

This research received no external funding.

References

1. UNCTAD. *Review of Maritime Transport 2025: Staying the Course in Turbulent Waters* (United Nations, Geneva, Switzerland, 2025). https://unctad.org/publication/review-maritime-transport-2025 (accessed 20 October 2026).

2. Sorte, S., Rodrigues, V., Borrego, C. & Monteiro, A. Impact of harbour activities on local air quality: a review. *Environ. Pollut.* **257,** 113542 (2020). https://doi.org/10.1016/j.envpol.2019.113542.

3. Yang, S. et al. Evaluating methods for marine fuel sulfur content using microsensor sniffing systems on ocean-going vessels. *Sci. Total Environ.* **942,** 173765 (2024). https://doi.org/10.1016/j.scitotenv.2024.173765.

4. Šaparnis, L., Rapalis, P. & Daukšys, V. Ship emission measurements using multirotor unmanned aerial vehicles: review. *J. Mar. Sci. Eng.* **12,** 1197 (2024). https://doi.org/10.3390/jmse12071197.

5. Shen, L., Sun, J. & Yang, D. Research on path optimization for collaborative UAVs and mothership monitoring of air pollution from port vessels. *Sustainability* **16,** 4948 (2024). https://doi.org/10.3390/su16124948.

6. Qi, Y. et al. Multi-UAV path planning considering multiple energy consumptions via an improved bee foraging learning particle swarm optimization algorithm. *Sci. Rep.* **15,** 14755 (2025). https://doi.org/10.1038/s41598-025-99001-z.

7. Ma, H. et al. Heterogeneous multi-UAVs cooperative task allocation based on the improved coati optimization algorithm. *Proc. Inst. Mech. Eng. G J. Aerosp. Eng.* **239,** 1843–1857 (2025). https://doi.org/10.1177/09544100251343664.

8. Ma, Z., Liu, W., Hu, C., Gong, H. & Wang, X. Path cooperative planning for unmanned aerial vehicles based on improved artificial bee colony algorithm. *J. Nanjing Univ. Aeronaut. Astronaut.* **57,** 1124–1134 (2025). (In Chinese). https://doi.org/10.16356/j.1005-2615.2025.06.009.

9. Liu, Y., Dong, H., Liu, H., Li, H. & Zhang, W. An improved PSO-ABC path planning algorithm for UAVs based on a construction of urban airspace topology with actual GIS data. *Sci. Rep.* **16,** 5048 (2026). https://doi.org/10.1038/s41598-026-35958-9.

10. Tong, M., Peng, Z. & Wang, Q. A hybrid artificial bee colony algorithm with high robustness for the multiple traveling salesman problem with multiple depots. *Expert Syst. Appl.* **260,** 125446 (2025). https://doi.org/10.1016/j.eswa.2024.125446.

11. Lindauer, M. et al. SMAC3: a versatile Bayesian optimization package for hyperparameter optimization. *J. Mach. Learn. Res.* **23**(54)**,** 1–9 (2022). https://www.jmlr.org/papers/v23/21-0888.html (accessed 20 October 2026).

12. Weiß, D., Schede, E. & Tierney, K. Selector: ensemble-based automated algorithm configuration. *J. Heuristics* **31,** 28 (2025). https://doi.org/10.1007/s10732-025-09561-6.

13. Anastacio, M., Matricon, T. & Hoos, H. H. Instance selection methods in automated algorithm configuration. *Eur. J. Artif. Intell.* https://doi.org/10.1177/30504554261453277 (2026). Advance online publication.

14. Korsah, G. A., Stentz, A. & Dias, M. B. A comprehensive taxonomy for multi-robot task allocation. *Int. J. Robot. Res.* **32,** 1495–1512 (2013). https://doi.org/10.1177/0278364913496484.

15. He, L. et al. A survey of normalization methods in multiobjective evolutionary algorithms. *IEEE Trans. Evol. Comput.* **25,** 1028–1048 (2021). https://doi.org/10.1109/TEVC.2021.3076514.

16. Miller, C. E., Tucker, A. W. & Zemlin, R. A. Integer programming formulation of traveling salesman problems. *J. ACM* **7,** 326–329 (1960). https://doi.org/10.1145/321043.321046.

17. Shi, Y. & Eberhart, R. A modified particle swarm optimizer. In *Proceedings of the 1998 IEEE International Conference on Evolutionary Computation* 69–73 (IEEE, Anchorage, AK, USA, 4–9 May 1998). https://doi.org/10.1109/ICEC.1998.699146.

18. Karaboga, D. & Basturk, B. A powerful and efficient algorithm for numerical function optimization: artificial bee colony (ABC) algorithm. *J. Glob. Optim.* **39,** 459–471 (2007). https://doi.org/10.1007/s10898-007-9149-x.

19. Rosenkrantz, D. J., Stearns, R. E. & Lewis, P. M., II. An analysis of several heuristics for the traveling salesman problem. *SIAM J. Comput.* **6,** 563–581 (1977). https://doi.org/10.1137/0206041.

20. Croes, G. A. A method for solving traveling-salesman problems. *Oper. Res.* **6,** 791–812 (1958). https://doi.org/10.1287/opre.6.6.791.

21. Hutter, F., Hoos, H. H. & Leyton-Brown, K. Sequential model-based optimization for general algorithm configuration. In *Learning and Intelligent Optimization* (ed. Coello Coello, C. A.) **6683,** 507–523 (Springer, Berlin/Heidelberg, Germany, 2011). https://doi.org/10.1007/978-3-642-25566-3_40.

22. Breiman, L. Random forests. *Mach. Learn.* **45,** 5–32 (2001). https://doi.org/10.1023/A:1010933404324.

23. Jin, Y. Surrogate-assisted evolutionary computation: recent advances and future challenges. *Swarm Evol. Comput.* **1,** 61–70 (2011). https://doi.org/10.1016/j.swevo.2011.05.001.

24. Beed, R., Roy, A., Sarkar, S. & Bhattacharya, D. A hybrid multi-objective tour route optimization algorithm based on particle swarm optimization and artificial bee colony optimization. *Comput. Intell.* **36,** 884–909 (2020). https://doi.org/10.1111/coin.12276.

25. Wang, Y. D. Synergistic path planning of multi-UAVs for air pollution detection of ships in ports. Master's thesis, Dalian Maritime University, Dalian, China (2021). (In Chinese).

675 26. Wu, X. W., Guo, M. Y., Hu, A. J. & Wu, Q. Path planning for UAV based on improved hybrid
676 genetic particle swarm algorithm. *Chin. J. Sci. Instrum.* **46,** 315–325 (2025). (In Chinese).
677 https://doi.org/10.19650/j.cnki.cjsi.J2413512.

678 27. Shen, L. et al. Synergistic path planning of multi-UAVs for air pollution detection of ships in ports.
679 *Transp. Res. E Logist. Transp. Rev.* **144,** 102128 (2020). https://doi.org/10.1016/j.tre.2020.102128.

680 28. Bergstra, J. & Bengio, Y. Random search for hyper-parameter optimization. *J. Mach. Learn. Res.*
681 **13,** 281–305 (2012). https://www.jmlr.org/papers/v13/bergstra12a.html (accessed 20 October
682 2026).

683 29. Welch, B. L. The generalization of 'Student's' problem when several different population variances
684 are involved. *Biometrika* **34,** 28–35 (1947). https://doi.org/10.1093/biomet/34.1-2.28.